Space- and time-resolved ion distribution in a recombining aluminum x-ray laser plasma

A. Klisnick,[1] C. Chenais-Popovics,[2] C. A. Back,[3] P. Zeitoun,[1] P. Renaudin,[2,*] O. Rancu,[2] J. C. Gauthier,[2] and P. Jaeglé[1]
[1]*Laboratoire de Spectroscopie Atomique et Ionique, CNRS URA 775, Université Paris-Sud, Bâtiment 350, 91405 Orsay Cedex, France*
[2]*Laboratoire pour l'Utilisation des Lasers Intenses, (LULI) CNRS UMR 100, Ecole Polytechnique, 91128 Palaiseau Cedex, France*
[3]*Lawrence Livermore National Laboratory, (LLNL) PO Box 808, Livermore, California 94551*
(Received 5 January 1996)

These experiments map out the ionization balance present in a recombination x-ray laser plasma as a function of time and space. The plasma is created by irradiating an Al strip target with a 600-ps Nd:glass laser, and is probed by an x-ray backlight at several times as it cools and recombines. The primary diagnostic is an x-ray spectrometer which spatially resolves the He-like to Be-like $K\alpha$ absorption spectra as a function of distance from the target surface. The experimental results indicate that the plasma ions important to the lasing are observed much farther from the target than expected from simulations. These results are consistent with x-ray gain measurements, and demonstrate the effect of non–local thermal equilibrium cooling on the ionization balance. [S1063-651X(96)11105-3]

PACS number(s): 42.55.Vc, 52.50.Jm, 32.30.Rj, 52.70.−m

I. INTRODUCTION

Recombination pumping in hydrogenic, lithiumlike and sodiumlike ions was recognized early as an attractive way to produce x-ray lasers with low energy input requirements. Gain coefficients of 1–4 cm^{-1} have been measured on several transitions ranging between 40 and 250 Å in plasma columns produced by irradiating a solid target with a cylindrically focused high-power laser beam [1]. However the achievement of a large gain-length product necessary to reach high brightness lasing emission has revealed difficulties for reasons which are only partially understood. On the other hand, some persistent disagreements between the predictions of numerical simulations and the experimental observations were reported. One of the most important is that simulations do not account for the gains observed in plasmas created by relatively long (600 ps–2 ns) pulses [2], whereas they satisfactorily reproduce results obtained with shorter pulses (2–100 ps) [3]. Although we have shown that variations of the laser illumination along the length of the plasma column can affect the observed amplification [4], they cannot fully explain the discrepancy between predicted and measured gains.

The existence of population inversions in recombination x-ray lasers relies on the three-body recombination of highly charged ions at low temperature. This can be achieved either by rapidly cooling an initially hot plasma, or by optical field-ionization (OFI) of a gas with a femtosecond laser beam [5]. For the lithiumlike laser with which this paper deals, the plasma is initially ionized up to the heliumlike ionization stage through heating by the driving laser, and then cools down after the laser pulse as it expands in vacuum. One of the basic conditions for population inversions to exist is that the plasma ionization stage remains significantly larger than its steady-state value during cooling. In the case of the lithiumlike laser, this means that the density of heliumlike ions must be larger than it would be if steady-state equilibrium with local electron density and temperature was reached. This situation can be achieved if the cooling rate of the plasma is large compared to the He-like recombination rate. This feature, which does not exist in collisionally excited x-ray lasers, has important implications. From the experimental point of view the observed gain is sensitive to both heating by the pump laser, which fixes initial conditions, and the cooling rate of the plasma. From the simulation point of view the precision of the calculated gain depends on both the description of the density/temperature evolution and on the ionization/recombination rates involving the lasing ions and adjacent species. Because of the non-steady-state nature of the evolution of the ionization state, any error made in one of these aspects is cumulative with time, and can lead to significant errors in calculated gains.

Since non-steady-state ionization dynamics is crucial to the efficiency of a recombination x-ray laser scheme, these experiments were designed to measure the ionization state of the plasma at times where cooling and recombination giving rise to lasing take place. Very few experiments [6,7] have been performed up to now that provide measurements of plasma quantities other than gain coefficients in plasmas relevant to recombination x-ray lasers. Here we have applied the technique of absorption spectroscopy on $K\alpha$ transitions to an x-ray laser aluminium plasma column produced by a 600-ps pulse, in conditions identical to those used for the x-ray laser experiments performed at the LULI laser facility. In those experiments, described in [4], a gain coefficient of 1 cm^{-1} was measured at a distance 450 μm from the target surface for the $3d$-$4f$ line at 154.6 Å in lithiumlike Al^{10+}. Furthermore, a gain was observed to last from 0.5 to 2 ns after the peak of the laser pulse. These results were not consistent with predictions that place the maximum gain 350 μm from the surface at a delay of 2.2 ns with respect to the laser pulse.

$K\alpha$ absorption spectroscopy is well suited to study these plasmas because it provides a direct probe of the ground state

*Permanent address: CEA-Centre d'Etudes de Limeil-Valenton, 94195 Villeneuve-Saint-George Cedex, France.

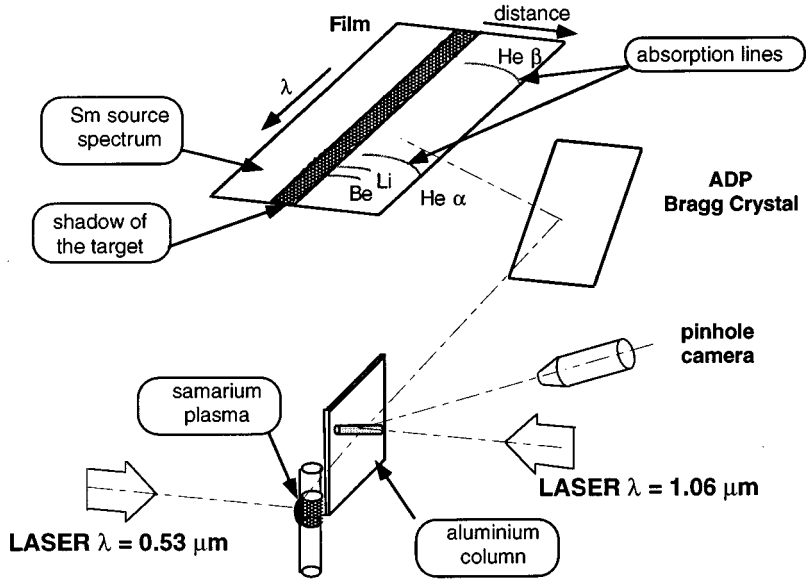

FIG. 1. Experimental setup showing the inclined position of the plasma column.

populations of the different ionic species present in the plasma. Under the conditions studied here the ground state population accounts for the bulk of the total population of the ionic species involved in the lasing process. To avoid changing plasma conditions important to achieving gain, we designed an experimental setup to enhance the visibility of the absorption structures from x-ray laser plasma columns without changing the target geometry. This setup is described in Sec. II. In Sec. III we present the absorption spectra obtained at three times during cooling of the x-ray laser aluminum plasma. Numerical simulations were performed to simulate the experimental results, yielding synthetic absorption spectra which are described in Sec. IV. A quantitative comparison of measured and calculated absorptions for He-, Li-, and Be-like ions is discussed in Sec. V. Conclusions are given in Sec. VI.

II. EXPERIMENTAL ARRANGEMENT

These experiments were performed using two beams of the LULI laser facility. Figure 1 shows the experimental setup. The primary beam ($\lambda=1.06$ μm, $1\omega_0$, pulse width 600 ps) was cylindrically focused onto a foil target with $(1-5)\times10^{12}$ W/cm^2 intensity to produce an Al plasma similar to those used in previous x-ray laser experiments described above. The length of the plasma column was adjusted to 10 mm by use of an aperture placed in front of the focusing system. This plasma column was probed by an x-ray backlight source that was generated by the second laser beam. This beam ($\lambda=0.53$ μm, $2\omega_0$, pulse width 600 ps) was spherically focused to $\sim5\times10^{14}$ W/cm^2 onto a 0.8-μm-thick samarium deposit, and was delayed relative to the primary beam.

The targets used to create the probed plasma were CH foils 50–75 μm thick, with a strip of Al 2000 Å thick and 70 μm wide coated on one side. The width of the focal line was approximately 100 μm, and overfilled the aluminum strip. The plasma formed from the strip has conditions similar to the lasing plasma, but is tamped on either side by CH to allow a better definition of the plasma transverse size giving the length probed by the backlight radiation. Further, the presence of the CH plasma restricts the transverse expansion of the aluminum column and reduces transverse gradients in the direction of probing by x rays. It was experimentally checked that this CH plasma does not introduce any additional absorption structures into the wavelength range of interest.

The primary diagnostic was an ammonium dihydrogen phosphate (ADP) Bragg crystal x-ray spectrometer that dispersed x rays onto direct x-ray film (Kodak SB392). The spectral resolution of $\sim$2000 allowed us to resolve the structure of the multiple transitions in the $K\alpha$ lines of different ionic species. The spectral resolution on film is given by the size of the backlight source, which was previously measured to be of the order of 20 μm [8]. The spectral resolution was hence limited to 4 mÅ in the 6–8 Å range. Other diagnostics included pinhole cameras and another imaging spectrometer to monitor the line-focus plasma and the backlight.

The setup, shown in Fig. 1, allows the plasma column to be probed in a direction perpendicular to the plasma expansion. The point projection backlight enables us to record data that are functions of wavelength in one direction and space in the perpendicular direction. Absorption lines are formed when backlight x-rays, having energies that correspond to Al $K\alpha$ transitions, are absorbed by the plasma being probed. The wavelength of the absorption lines identify the ion that is in absorption, while the position and length along the spatial axis of the film correspond to the distance from the target surface where the ion species is located. The temporal duration of the backlight source is 600 ps, and the absorption is recorded only during this period of time.

Absorption spectroscopy on $K\alpha$ transitions was previously developed for point plasmas [8,9] as well as for x-ray laser plasmas produced by short (100-ps) pulses [6]. However, the application of the $K\alpha$ absorption technique to a line-focus plasma required special adaptations. First, to ensure that the geometry of the plasma expansion is close to that of x-ray laser experiments, the length of the plasma gain medium must be kept longer than a few mm. Hence probing the plasma along its gain axis is not practical because it

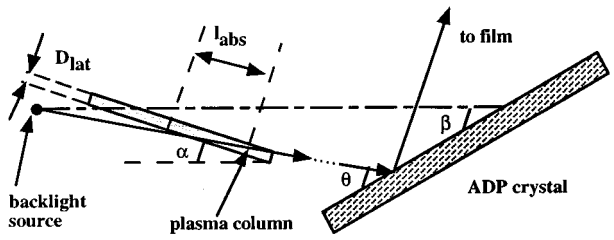

FIG. 2. Geometry of probing of the inclined plasma column by backlight radiation.

subtends a solid angle that is too small to probe a sufficient range of ionic species with the backlight.

The most straightforward experimental setup would probe the plasma column along its diameter. However, preliminary experiments indicated that the absorption length along this line of sight was not sufficient to produce a detectable absorption signal. Hence the plasma column was tilted to increase the absorption length without modifying the plasma conditions of importance to x-ray lasing. In this geometry, which is shown in Figs. 1 and 2, the path length of the C-like to Li-like $K\alpha$ transitions can be increased more than that of the He-like resonance line which yields a stronger absorption signal, because it has a much stronger oscillator strength and originates from the most abundant ionic species in the plasma.

In the experiment the plasma column was set at 18.8° by orienting the strip target through a microscope objective and aligning the focal line on this axis. The crystal in the spectrometer was set at 38.5° relative to the horizontal axis which defined the wavelength of the Al He_β ($1s^2$-$1s3p$) transition at 6.63 Å to be along the horizontal. This alignment procedure allowed us to probe the same length of plasma reproducibly from shot to shot.

The inclined configuration of the probed plasma introduces a wavelength dependence of several quantities: the absorption length l_{abs} of the backlight radiation, the position of probing z along the Al plasma axis, and the magnification M between the film plane and the plasma expansion axis. These quantities depend on wavelength λ because each wavelength probes the plasma column at a slightly different angle.

This point is illustrated in Fig. 2. Radiation of wavelength λ traveling through the plasma column is reflected by a crystal at a Bragg angle of θ. Hence the length of plasma traversed by the backlight, $l_{abs}(\lambda)$, is related to the transverse

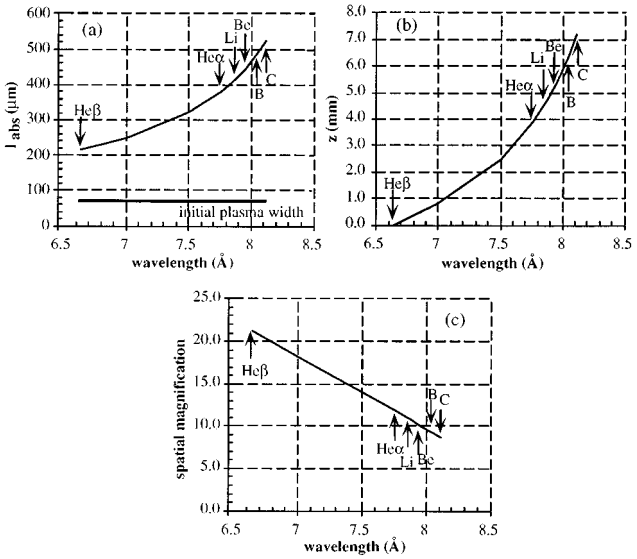

FIG. 3. The absorption length l_{abs} (a), the position z probed along the plasma column (b), and the spatial magnification (c) as functions of the wavelength of the backlight radiation.

size D_{lat} of the plasma column by the relation

$$l_{abs}(\lambda)=\frac{D_{lat}}{\sin(\alpha+\beta-\theta)}, \tag{1}$$

where α and β are the angles between the horizontal axis and the plasma column axis or the crystal surface, respectively (see Fig. 2). D_{lat} is given by the width of the Al column, that is initially 70 μm and increases with time and distance from the target. θ is the Bragg angle for the wavelength λ, and is given by

$$\theta=\mathrm{Arcsin}\left(\frac{\lambda}{2d}\right), \tag{2}$$

with $2d=10.648$ Å for the ADP crystal used in this experiment. Note that relation (1) is valid if θ greater than $\alpha+\beta$, which corresponds to λ smaller than 8.96 Å.

The graphs of Figs. 3(a)–3(c) show the dependence of the absorption length l_{abs}, the probing position z, and the spatial magnification M, in the spectral range including all $K\alpha$ transitions from He- to C-like species and the He_β line. The absorption length l_{abs} [Fig. 3(a)] increases from 380 μm at

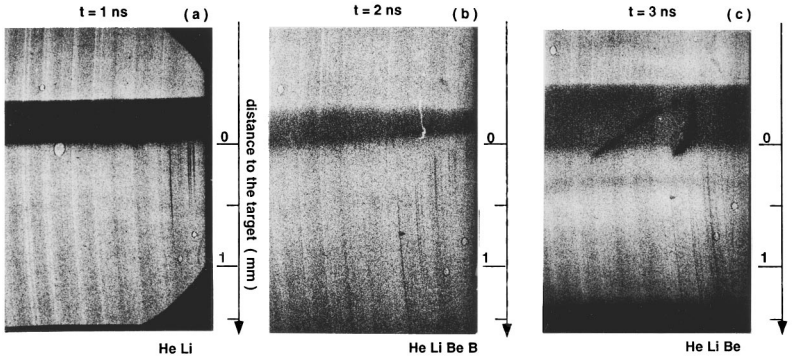

FIG. 4. Photographs of the samarium spectra, taken at $t=1$, 2, and 3 ns, respectively, after the peak of the pulse that created the probed aluminum plasma. Absorption structures corresponding to Al $K\alpha$ transitions are in the 7.7–8.2 Å wavelength range. The spatial scale has been drawn assuming a constant magnification of 10.

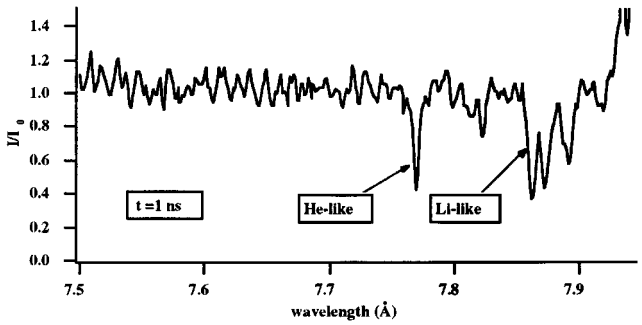

FIG. 5. Spectral lineout of the absorption spectrum at 1 ns, traced at 200 μm from the target surface and integrated over 250 μm.

7.75 Å, the wavelength of the He_α line, up to 523 μm at the position of the C-like $K\alpha$ lines located at approximately 8.1 Å. If $z=0$ is defined to be the position along the plasma column that corresponds to absorption of the Al He_β line, one can see in Fig. 3(b) that Al $K\alpha$ absorption of the He- to C-like ions is 4–7 mm farther along the axis of the plasma column. The magnification M [Fig. 3(c)] decreases with increasing wavelength and varies between 11.8 and 8.6 along the $K\alpha$ series. For the specific case of the He_α line (7.755 Å), a distance of 100 μm from the target corresponds to 1.2 mm on film along the spatial resolution axis.

III. SPATIAL DEPENDENCE OF THE PLASMA IONIZATION STATE AT DIFFERENT TIMES

The experimental data in Fig. 4 are typical of what was obtained for a series of shots using three different backlight delays, $t=1$, 2, and 3 ns. For this paper, $t=0$ is defined as peak of the $1\omega_0$ pulse that created the probed aluminium plasma. The shadow of the aluminium target appears in the center of each spectrum. The spectrum in the upper part corresponds to unabsorbed samarium radiation that passed behind the target. The lower part shows the spectrum of the samarium radiation transmitted through the aluminium plasma. The fine dark absorption lines which appear on the Sm emission correspond to the $K\alpha$ absorption transitions. Absorption lines belonging to He-, Li-, Be-, and B-like ionic species are the most prominent. The spatial extension along the direction perpendicular to the target surface varies for each ionic species and with time.

As discussed above, the geometrical configuration of the experiment includes the He_β absorption line on the same film as the $K\alpha$ lines. However, even when the He_β line was observed, it was too weak to be analyzed.

An example of a spectral lineout is shown in Fig. 5. Here the relative intensity as a function of wavelength is taken from the data in Fig. 4(a), where the He-like ions give a maximum absorption. It is taken at 200 μm from the surface and integrated over 250 μm, which is of the order of the spatial blurring introduced by the 600-ps probe duration. The nonabsorbed backlight intensity $I_0(\nu)$ is measured behind the target (top of the photographs of Fig. 4), and is corrected for the spatial variation of the source. The film background is measured in the shadow of the target and corrected for film imperfections.

The location of the absorbing ion species can be estimated from the data in Fig. 4. In each spectrum the spatial scale has been drawn using a constant magnification of 10, which corresponds to the average calculated value in the spectral range shown [Fig. 3(c)]. At a time 1 ns, only He- and Li-like absorption structures are in the observed spectral window. They extend from almost the target surface up to 700 or 500 μm, respectively. In Fig. 4(b), at a time 2 ns, the four groups of He-, Li-, Be-, and B-like absorption lines are observed. The He- and Li-like lines appear farther from the target surface than at $t=1$ ns, while the lines belonging to lower ionization stages, from Be-like up to C-like ions, are visible in a region gradually closer to the target. By 3 ns the He-like ions are still present quite far from the target surface. However, the He- and Li-like lines are much weaker than at $t=2$ ns, while the strongest ions in absorption are the Be-like ions.

Figure 6 shows a plot of the onset of the ionic species versus distance from the target at the three times studied. One can see that the He- and Li-like species become more and more detached from the surface for later times. An important fact to note is the presence of He-like ions later than 2 ns after the laser pulse, which is direct evidence of a non-steady-state ionization balance. Due to the expansion, the plasma density is no longer high enough to favor three-body recombination, and the plasma must radiatively recombine on characteristic time scales that are much longer. The He-like ion state is ''frozen in'' far from the target surface, while lower ionization stages are present closer to the target where the electron density is high enough for recombination to be efficient.

IV. NUMERICAL MODELING OF THE PLASMA IONIZATION STATE AND ABSORPTION SPECTRA

The experimental data were compared to theoretical predictions of the space and time evolutions of the plasma ionization state and of absorption spectra. The evolution of the aluminum plasma column created with conditions of irradiation similar to the experiments was calculated using the one-dimension hydrocode FILM in a 1.5-dimension geometry which includes a self-similar description of the lateral expansion of the plasma column [10]. In this calculation the evolution of the 70-μm aluminium strip deposited on mylar and irradiated with a 100-μm-wide focal line was designed to

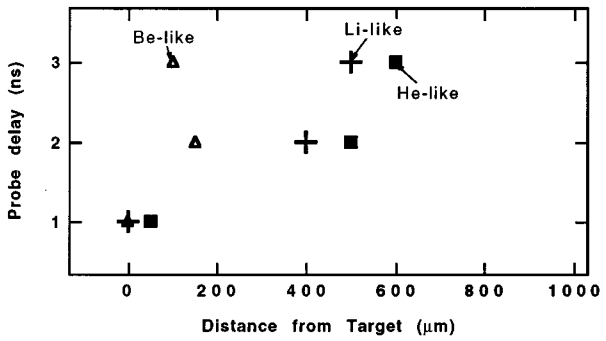

FIG. 6. The position of the ionic species plotted for the three probe delay times. The absorption for each species begins at the positions indicated on the graph, and extends away from the target surface which is located at $x=0$.

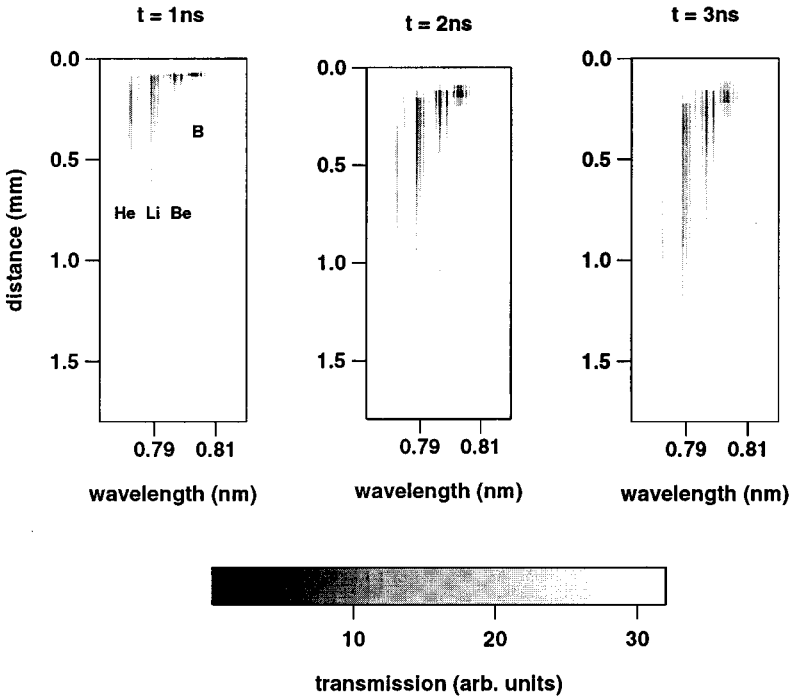

FIG. 7. Synthetic spectra showing the transmission on the $K\alpha$ lines as a function of the distance to the target surface at $t=1$, 2, and 3 ns.

match that of a pure aluminum target irradiated with a 100-μm focal width. The hydrodynamical evolution of the aluminium plasma is not expected to be perturbed by the presence of the mylar plasma.

The code FILM provides the temporal and spatial variation of several plasma quantities, such as electron density and temperature, as well as of the fractional abundances of the ionic species present in the plasma. The calculation of the ionization dynamics is performed with a time-dependent model [11] and the contribution of the He- and Li-like excited levels is included via quasi-steady-state effective rates [2,12,13]. For all other species, from neutral atom to Be-like ions, only the ground state is included. A more detailed description of this model can be found in [2,11].

The radiation intensity measured on the x-ray film is given by

$$I(\lambda)=I_0(\lambda)\exp[-\tau(\lambda)]+I_{\rm emis}+I_{\rm backg},$$

where $\tau(\lambda)=K(\lambda)l_{\rm abs}(\lambda)$ is the optical depth for each absorption line, $I_0(\lambda)$ is the Sm backlight intensity transmitted through the plasma, $I_{\rm emis}$ is the self-emission from the plasma, and $I_{\rm backg}$ is the background intensity level on the film. The two quantities appearing in the optical depth depend on both time and spatial position along the expansion axis. The backlighter intensity $I_0(\lambda)$ and the background intensity $I_{\rm backg}$ can be determined directly on the x-ray film (see Fig. 1). The self-emission from the plasma, which is time integrated over the whole duration of the probed plasma, can be measured in the backlighter-induced shadow of the target. It was found to be negligible at the low laser irradiances used in the present study. We note that any line emission would have appeared at wavelength positions slightly displaced from the position of the absorption lines because the wavelength dispersion in the film plane is different for emissions originating from the backlighter and plasma planes.

The absorption length $l_{\rm abs}$ has been calculated from the transverse size $D_{\rm lat}$ of the plasma given by the code FILM, taking into account the wavelength dependence given by relation (1). $D_{\rm lat}$ is also corrected by a reduction factor 70/100 to account for the fact that the initial width of aluminum is 70 μm in the experiment, while the focal spot in the experiment and simulations is 100 μm.

An absorption model is used to calculate the transmission I/I_0 of the $K\alpha$ transitions for the ionic species present in the plasma. The absorption coefficient is given by

$$K(\nu)=(c^2/8\pi)A_{ji}\,\frac{g_j}{g_i}\,N_j\,\frac{\phi(\nu)}{\nu^2},$$

where c is the light speed, A_{ji} are the transition probabilities, and g_i and g_j are the atomic weights calculated with the atomic structure code RELAC [14], N_j is the population of the ground level of the transition under study, and $\Phi(\nu)$ is the absorption line profile. The population of the closely lying levels that can serve as the lower state of the absorption transition are assumed to be in local thermodynamic equilibrium (LTE) with the ground state. The line profile $\Phi(\nu)$ was a Voigt profile with a Lorentzian contribution including the natural and autoionization width, and a Gaussian contribution due to a Doppler width. The Sm transmission I/I_0 has finally been convolved with a 1-eV Gaussian instrumental profile. The temporal duration of the backlight is included in the calculation of the synthetic spectra by integrating the transmission over the duration of the backlight pulse.

Figure 7 shows the reconstructed transmission spectra calculated at the three temporal delays shown in Fig. 4, $t=1$, 2, and 3 ns. The four groups of absorption lines belonging to He-, Li-, Be-, and B-like ionic species can be observed. The spectra are cut off at the outer edge of the plasma simulation at distances of 0.6, 1.2, and 1.5 mm for the respective times shown. General trends of the experimental images of Fig. 4 are well reproduced by the calculation. The location of the

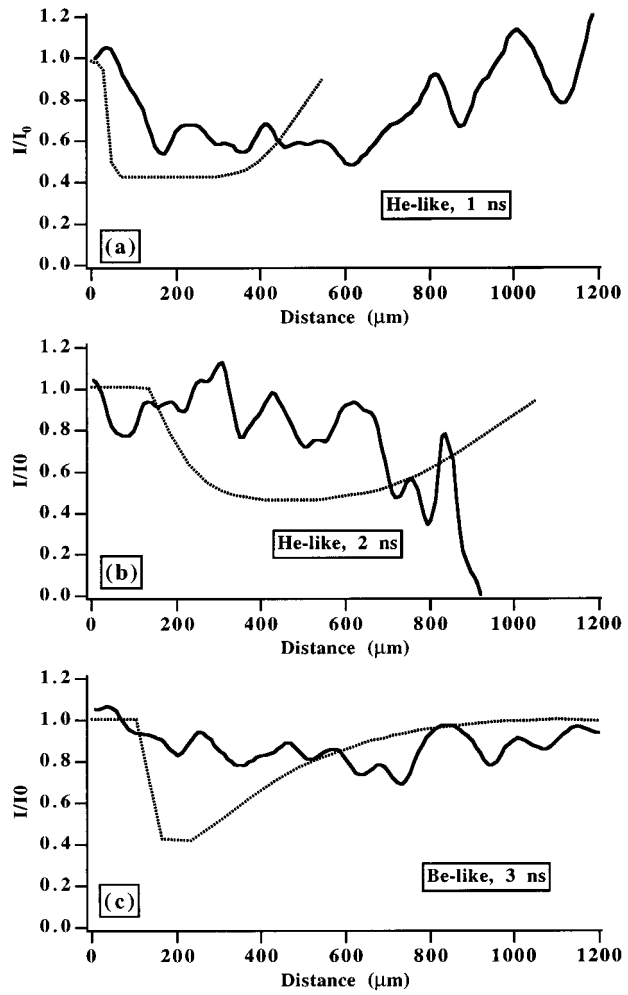

FIG. 8. Transmission as a function of the distance from the target for three cases: (a) He_α at 1 ns, (b) He_α at 2 ns, and (c) Be-like $K\alpha$ at 3 ns. Dotted line: calculation from the hydrocode FILM. Thick line: experimental data.

He- and Li-like species extend up to the limit of the plasma simulation, whereas the less ionized species exist in a region closer to the target surface, as observed in the experimental spectra. The He-like ions move away from the target surface as a function of time after the laser pulse ends.

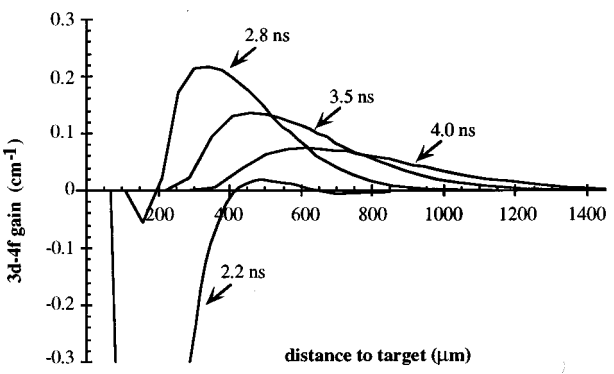

FIG. 9. Calculated $3d$-$4f$ gain vs distance from the target at different times between 1.4 and 3.6 ns.

A more detailed comparison of the location and extension of each ionic species reveals that the distances calculated by the simulations are generally smaller than those observed in the experimental spectra. For example, at $t=2$ ns. He-like ions extend from 200 μm to 1 mm on the synthetic spectrum, whereas the observed positions are 500 μm to more than 1.5 mm on the experimental spectrum. The other point which has to be noted is that, at $t=3$ ns, simulation predicts that He- and Li-like ions are still abundant in the plasma, since they yield the strongest absorption lines in Fig. 7(c). However, the experiment shows that Be-like ions are dominant at that time, while the He- and Li-like species are strikingly weak. A quantitative comparison of the absorptions of He- and Be-like ions as a function of space is presented and discussed in Sec. V.

V. QUANTITATIVE ANALYSIS AND DISCUSSION OF THE RESULTS

Figure 8 shows a selection of calculated and measured transmissions I/I_0 plotted as a function of the distance to the target. The absorption on the He_α line is represented at $t=1$ and 2 ns in Fig. 8(a) and 8(b), respectively. Figure 8(c) shows the absorption on the strongest Be-like transition at $t=3$ ns. The calculated transmission curves were obtained from the plasma parameters given by FILM, using basically the same method as described in Sec. IV.

In Fig. 8(a) the experimental curve shows that, at $t=1$ ns, the He-like ions absorb mainly between 100 and 700 μm from the target surface, whereas calculations predict that they absorb between 50 and 500 μm. The experimental transmission I/I_0 reaches a minimum value of (0.6 ± 0.1). The calculated value is slightly less (0.45). The main discrepancy is in that the experimental positions of absorption are farther from the target surface than predicted by the simulations.

At 2 ns, the disagreement between experiments and simulations becomes more pronounced. On the He-like line the experimental transmission [Fig. 8(b)] remains close to unity near the target, and decrease from 500 μm. The absorption value away from the target is difficult to measure because of large fluctuations of I/I_0 due to the weakness of the signal on film. In comparison, the code predicts that the He-like absorbing region lies closer to the target, with a peak of absorption at 400 μm.

It is important to note here that the disagreement between theory and experiment on the positions of He- and Li-like ions is consistent with the measurements of the position of the maximum gain on the Li-like $3d$-$4f$ line. As recalled in the beginning of this paper, gain on this line was measured at 450 ± 100 μm from the target surface from 0.5 to 2 ns after the peak of the laser pulse. In comparison, simulations predict that the gain exists from 1.6 ns up to more than 3.6 ns, and maximizes at 2.2 ns in a region centered at 350 μm from the target surface, as shown in Fig. 9. The present experiment, however, shows [Figs. 4(b) and 8(b)] that, at a time 2 ns, the He- and Li-like ions of importance for lasing are present farther from the target. The location of He- and Li-like ions measured from the experimental absorption spectra is thus in contradiction with the position of the gain region predicted by the code, but it is consistent with previous gain measurement.

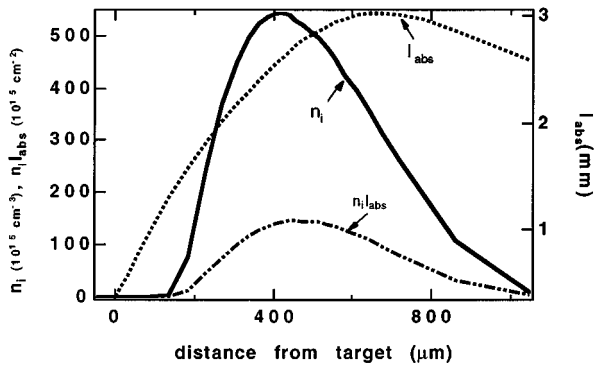

FIG. 10. The ionic population, absorption length, l_{abs}, and the product of these two quantities for He-like ions at 2 ns after the driving laser pulse.

Finally, at $t=3$ ns, Be-like ions are measured to absorb over the whole spatial region covered by the experiment, with a minimum transmission of 0.7 while the calculated transmission shows a minimum value of 0.4 at 200 μm from the target [Fig. 8(c)]. At distances from the target larger than 500 μm, the absorption by Be-like ions is much stronger in the experiment than in the simulation.

This indicates that the recombination from Li- to Be-like ions in the plasma corona is probably underestimated in our modeling. The ionization kinetics in FILM includes the contribution of excited levels to ionization and recombination for He- and Li-like ions only using quasi-steady-state effective rates [2,12,13]. For the description of lithiumlike recombination x-ray lasers, the inclusion of a sufficiently large number of lithiumlike excited levels in the heliumlike ion recombination process was found to be essential. This is mainly because at low temperature three-body recombination into the Li-like highly excited levels dominates over radiative recombination to the ground state. Neglecting the contribution of Li-like excited levels led to an erroneously low recombination rate and to a completely frozen ionization state during plasma cooling. Recombination and ionization from and to lower ionic species still only involve ground states. The disagreement observed at $t=3$ ns clearly demonstrates that the use of effective rates should be extended to other ionic species. In particular, the results shown here indicate that the recombination to the Be-like stage may require an effective rate that is much larger.

Overall, the discrepancy between simulations and experiment on the position and extension of the absorbing zones could be attributed to a poor description of either the plasma expansion or the ionization dynamics or to both of them. Although these two effects cannot be separated, the simulations give us some insight into the problem.

First, analysis of the simulations shows that the absorption near the target surface can always be correlated to the peak in the ionic population. In Fig. 8, the simulated transmission curves are calculated from the product $N_i l_{\mathrm{abs}}$, i.e., the ionic species density times the absorption length. Figure 10 shows the population and absorption length plotted individually, as well as the product of these two quantities, for the He-like stage in the $t=2$-ns case. One can see that the absorption close to the target surface is dominated by the ionic distribution. While the exact value of the plasma line width, from which l_{abs} is calculated, is difficult to verify experimentally, it is unphysical to expect it to decrease as a function of distance from the target. Similarly the quantity l_{abs} must increase as a function of time since the plasma is expanding. The absorption length modifies this distribution, but is not sufficient to bring the calculation into agreement with the experiment.

Second, simulations were used to explore the sensitivity of the calculated transmission spectra to laser intensity variations. As noted above, the uniformity of the line focus was monitored by emission from an independent spectrometer that imaged the plasma along its length. This spectrometer was positioned face on to the line focus and spatially resolved the emission of the He- and H-like lines along the plasma axis. The He-like Al lines were weakly visible, and the H-like lines were absent on typical shots. The images were formed by the plasma in emission, and show intensity variations that had a large-scale structure with a period of 800 μm. The variations in intensity lineouts of the Al He_α line were $<20\%$ along the length of the plasma focus. Pinhole images obtained from a coupled charge device (CCD) also confirmed this weak intensity variation along the plasma length.

Based on these measurements, several simulations were performed varying the nominal laser intensity of 1.6×10^{12} W/cm^2. Changes of up to 20% in the laser intensity do change the total population of the ionic species by approximately 15%. However, they do not change the expansion of the plasma significantly, and hence, the peak position of the ionic species as a function of time is not significantly affected. Thus laser intensity variations along the focal line cannot explain the discrepancy between the simulations and experiments.

Therefore, the disagreement between the experimental results and the simulations is primarily due to difficulties calculating the spatial distribution of N_i. While these results do not directly suggest ways to experimentally improve the gain of recombination x-ray lasers, they do help us understand why the longer ns pulses do not produce the predicted gain. The results also show that a better description of recombining plasmas is clearly necessary for the design of more efficient x-ray lasers of this kind.

VI. CONCLUSIONS

This study focuses on He-, Li-, and Be-like ionic species, since these are the most important to x-ray laser schemes in Li-like recombination lasers. The ionization balance is difficult to calculate because the recombination is extremely sensitive to the level of atomic detail used in the kinetics model as well as the plasma cooling rate. In the experiment, we have been able to map out the spatial position of the ionic species as a function of time by absorption spectroscopy.

The production of a significant gain region in recombination x-ray lasers depends strongly on the homogeneity of the plasma, and on rapid cooling to create the population inversions. An important aspect of the time-dependent non-LTE model is confirmed in these experiments because it is clear that the He-like ions do not cool as a steady-state model would predict. The He-like ion is experimentally shown to exist far from the target ($z>500$ μm) and late in time ($t\approx3$ ns). This is a clear evidence of a non-LTE frozen ionization state.

Our measurements show that the He- and Li-like ground state ions are farther away from the target than predicted by the simulations by a factor of ~2. These results are consistent with gain measurements done under similar laser and target conditions where the gain region was found to be ~450 μm from the target surface at a time between 0.5 and 2.0 ns after the heating laser pulse.

An investigation of the simulations shows that discrepancies between the data and calculations on the position and extension of the absorbing zones can be attributed to errors in calculating the spatial distribution of the ionic populations. Two different aspects of the model could be suspected: (i) a description of the plasma hydrodynamics giving the spatial distributions of density and temperature, or (ii) the rates of ionization and recombination which govern the existence of the ionic species. Further research should discriminate between these two aspects by measuring another plasma quantity, such as the electron density. In addition, the predominance of Be-like ions at a late time indicates that the rate of recombination to Be-like states is still not well modeled. While the improvements to the model have helped, they are still not adequate. Further work should focus on these different aspects to understand better plasmas with densities lower than 10^{21} cm^{-3}.

ACKNOWLEDGMENTS

We would like to thank the technical support of the LULI technical staff, in particular R. Konig, and also J. C. Lagron and L. Vanbostal at the Laboratoire de Spectroscopie Atomique et Ionique. We also thank the ''Laboratoire des cibles'' at the Institut de Physique Nucléaire and Ed Hsieh of LLNL target fabrication for producing the targets and S. Equilbey at the Centre de Densitométrie de l'Institut d'Optique in Paris-Sud University for his help in data digitization.

[1] A review of results obtained by different laboratories can be found in *X-Ray Lasers 1994*, edited by D. Eder and D. Matthews, AIP Conf. Proc. No 332 (AIP, New York, 1994).

[2] A. Klisnick, A. Sureau, H. Guennou, C. Möller, and J. Virmont, Appl. Phys. B **50**, 153 (1990).

[3] P. B. Holden, S. B. Healy, G. J. Pert, M. H. Key, and J. Zhang, J. Phys. B **28**, 2745 (1995).

[4] P. Zeitoun, G. Jamelot, A. Carillon, P. Goedtkindt, H. Guennou, P. Jaeglé, A. Klisnick, C. Möller, B. Rus, and A. Sureau, in *X-Ray Lasers 1994*, edited by D. Eder and D. Matthews, AIP Conf. Proc. No 332 (AIP, New York, 1994), p. 55.

[5] Y. Nagata, K. Midorikawa, S. Kubodera, M. Obara, H. Tashiro, and K. Toyoda, Phys. Rev. Lett. **71**, 3774 (1993).

[6] D. O'Neill, C. L. S. Lewis, D. Neely, and S. J. Davidson, Phys. Rev. A **44**, 2641 (1991).

[7] J. C. Kieffer, M. Chaker, H. Pépin, H. A. Baldis, G. D. Enright, B. Lafontaine, and D. M. Villeneuve, Phys. Fluids B **3**, 463 (1991).

[8] C. A. Back, C. Chenais-Popovics, P. Renaudin, J. P. Geindre, P. Audebert, and J. C. Gauthier, Phys. Rev. A **46**, 3405 (1992).

[9] S. Gary, J. Bruneau, A. Decoster, D. Desenne, F. Garaude, J. P. LeBreton, J. C. Gauthier, J. Bauche, C. Bauche-Arnoult, J. L. Ocana, C. Molpeceres, and M. L. Gomez, J. Quantum. Spectrosc. Radiat. Transfer **54**, 155 (1995).

[10] A. Klisnick, J. Virmont, N. Grandjouan, A. Sureau, H. Guennou, in *X-Ray Lasers 1992*, edited by E. E. Fill, IOP Conf. Proc. No. 125 (Institute of Physics and Physical Society, Bristol, 1992), p. 305.

[11] J. C. Gauthier, J. P. Geindre, N. Grandjouan, and J. Virmont, J. Phys. D **16**, 321 (1983).

[12] P. Alaterre, Ph.D. thesis, Paris-Sud University, 1984 (in French).

[13] P. Audebert, Ph.D. thesis, Paris-Sud University, 1985 (in French).

[14] E. Luc-Koenig, Phys. Scr. **62**, 393 (1972); M. Klapish, J. L. Schwob, B. S. Fraenkel, and J. Oreg, J. Opt. Soc. Am. **67**, 148 (1977).